RESIDUAL STRENGTH PRESSURE TESTS AND NONLINEAR ANALYSES OF STRINGER- AND FRAME-STIFFENED ALUMINUM FUSELAGE PANELS WITH LONGITUDINAL CRACKS

Richard D. Young, Marshall Rouse, Damodar R. Ambur and James H. Starnes, Jr.
NASA Langley Research Center
Hampton, VA

Presented at the Second Joint DoD/FAA/NASA Conference on Aging Aircraft
Williamsburg, VA
August 31-September 3, 1998

RESIDUAL STRENGTH PRESSURE TESTS AND NONLINEAR ANALYSES OF STRINGER- AND FRAME-STIFFENED ALUMINUM FUSELAGE PANELS WITH LONGITUDINAL CRACKS

Richard D. Young, Marshall Rouse, Damodar R. Ambur, and James H. Starnes, Jr.
NASA Langley Research Center
Hampton, VA 23381
Tel: 757-864-2894
Fax: 757-864-7791
r.d.young@larc.nasa.gov

ABSTRACT

The results of residual strength pressure tests and nonlinear analyses of stringer- and frame-stiffened aluminum fuselage panels with longitudinal cracks are presented. Two types of damage are considered: a longitudinal crack located midway between stringers, and a longitudinal crack adjacent to a stringer and along a row of fasteners in a lap joint that has multiple-site damage (MSD). In both cases, the longitudinal crack is centered on a severed frame. The panels are subjected to internal pressure plus axial tension loads. The axial tension loads are equivalent to a bulkhead pressure load. Nonlinear elastic-plastic residual strength analyses of the fuselage panels are conducted using a finite element program and the crack-tip-opening-angle (CTOA) fracture criterion. Predicted crack growth and residual strength results from nonlinear analyses of the stiffened fuselage panels are compared with experimental measurements and observations. Both the test and analysis results indicate that the presence of MSD affects crack growth stability and reduces the residual strength of stiffened fuselage shells with long cracks.

1. INTRODUCTION

The fail-safe design philosophy applied to transport aircraft fuselage structures requires that the structures retain adequate structural integrity in the presence of discrete source damage or fatigue cracks. As economic factors encourage the use of commercial and military transport aircraft well beyond their original design requirement, it has become increasingly important to develop methods to predict accurately the residual strength of structures with cracks. The goal of NASA's Aircraft Structural Integrity Program is to develop a verified nonlinear structural analysis methodology for stiffened structures with damage and subjected to combined internal pressure and mechanical loads. The approach to accomplish this goal has been to: develop hierarchical modeling strategies required to represent the multi-dimensional length scales present in fuselage shells with cracks and multiple-site damage (MSD); develop material and geometric nonlinear shell analysis capabilities and conduct nonlinear analyses of stiffened shells subjected to internal pressure and mechanical loads; and conduct experiments to verify analyses and to identify critical behavioral characteristics.

The present paper presents recent results of residual strength pressure tests and nonlinear analyses of stringer- and frame-stiffened aluminum fuselage panels with longitudinal cracks. The tests and analyses, performed by the Structural Mechanics Branch at the NASA Langley Research Center, were intended to verify the analyses methods and to identify critical behavioral characteristics of the crack growth in generic wide-

body fuselage panels with long cracks. Two damage conditions are considered: a longitudinal crack located midway between stringers, and a longitudinal crack adjacent to a stringer and along a row of fasteners in a lap joint that has multiple-site damage (MSD). The loading condition for the panels is internal pressure plus axial tension loads. The axial tension loads are equivalent to a bulkhead pressure load. The fuselage panel tests are described and experimental results are reported. Then, analysis and finite element modeling methods using the STructural Analysis of General Shells (STAGS) program[1] are described. A description of the crack-tip-opening-angle (CTOA) skin fracture criterion[2,3] and the procedure for defining fracture parameters based on small laboratory specimens are presented. Predicted crack growth and residual strength results from nonlinear analyses on the stiffened fuselage panels are then compared with experimental measurements and observations.

2. EXPERIMENTS

Two stringer- and frame-stiffened aluminum fuselage panels with longitudinal cracks were tested in the pressure-box test machine at NASA Langley Research Center. The test specimens, the test machine, and the test method, are described. Then, the test results are presented.

2.1 TEST SPECIMENS

The first fuselage panel tested in this study, ASIP1, has six stringers and three frames, and is shown in Fig. 1 prior to testing. The overall dimensions of the panel include a 122-in. radius, a 72-in. length, and a 63-in. arc width. The skin is 0.063-in.-thick 2024-T3 aluminum with the sheet rolling direction parallel to the stringers. The stringers are 7075-T6 aluminum Z-section stringers with a stringer spacing of 8.1 in. The frames are 7075-T6 aluminum I-section frames with a frame spacing of 22 in. There are 0.063-in.-thick 2024-T3 aluminum circumferential tear straps, bonded to the skin, and located midway between the frames. The stringers and frames are riveted to the skin, and the frames are connected to the stringers by riveted stringer clips. Aluminum doublers are fastened to the curved ends of the panel between the stringers and along the sides of the panel between the frames. These doublers distribute the loads from the axial and hoop load plates into the panel skin, and they are slotted to be flexible in the direction parallel to the panel edges. The initial damage for panel ASIP1 was a 10-in.-long longitudinal crack, located midway between stringers and centered on a severed frame, as indicated in Fig. 1.

The second fuselage panel tested in this study, ASIP2, has four stringers and three frames, and is shown prior to testing in Fig. 2(a). The overall dimensions of this panel are the same as for ASIP1: a 122-in. radius, a 72-in. length, and a 63-in. arc width. The skin is 0.063-in.-thick 2024-T3 aluminum with the sheet rolling direction parallel to the stringers. The stringers are 2024-T3 aluminum inverted hat-section stringers with a stringer spacing of 14 in. The frames are 2024-T3 aluminum Z-section frames with a frame spacing of 22 in. There are 0.040-in.-thick 2024-T3 aluminum waffle tear straps, bonded to the skin, and located under the stringers and frames, but there are no tear straps midway between the frames. The stringers and frames are riveted to the skin and tear straps, and the frames are connected to the stringers by riveted stringer clips. Aluminum doublers are fastened to the curved ends of the panel between the stringers and along the sides of the panel between the frames to distribute the loads from the axial and hoop load introduction plates into the panel skin. There is a lap joint in this panel under the second stringer from the left as the panel is shown in Fig. 2(a). In the lap joint, the skin from the right side of the panel is the outer skin and overlaps at a greater radius over the inner skin from the left side of the panel. The layers of the lap joint are connected with three rows of 0.125-in.-diameter countersunk fasteners. The fastener pitch in the longitudinal direction is 1.0 in., and the three rows of fasteners are spaced 1.33 in. in the circumferential direction with the middle row of fasteners centered on a hat-section stringer. The initial damage for panel ASIP2 consisted of a 10-in.-long longitudinal lead crack and MSD cracks along the edge of the lap joint. The 10-in.-long lead crack was located adjacent to the second stringer and centered on a severed frame, as indicated in Fig. 2(a). A schematic

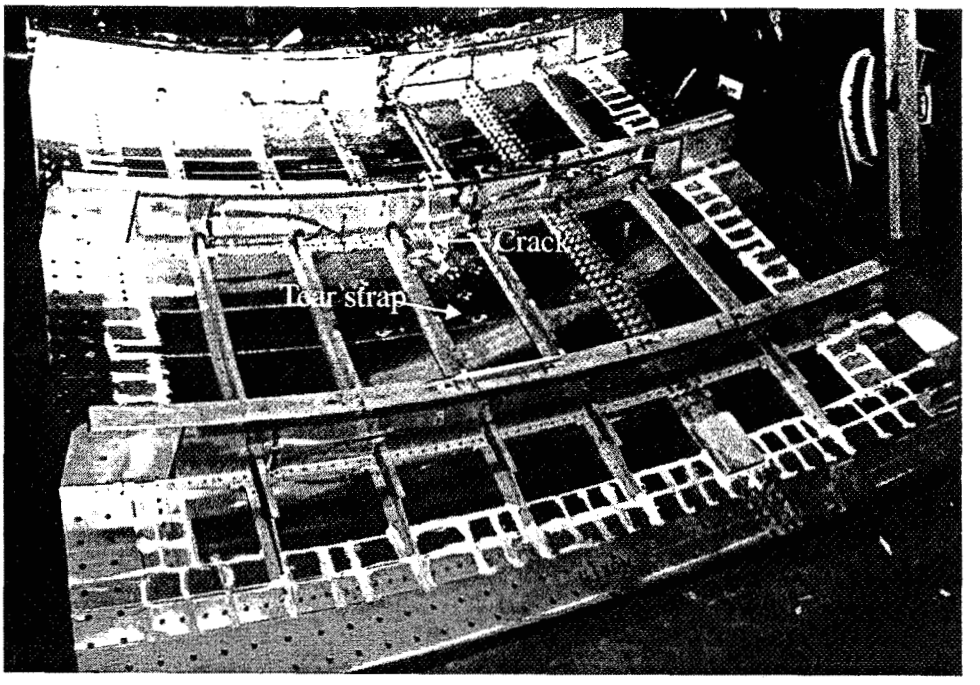

Figure 1. Panel ASIP1 prior to testing.

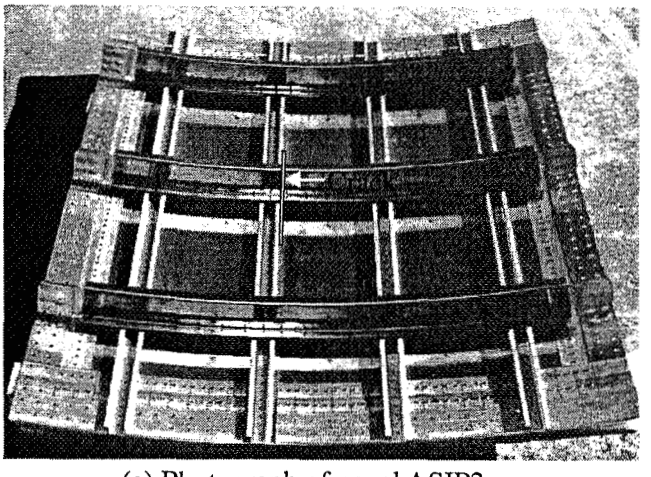

(a) Photograph of panel ASIP2

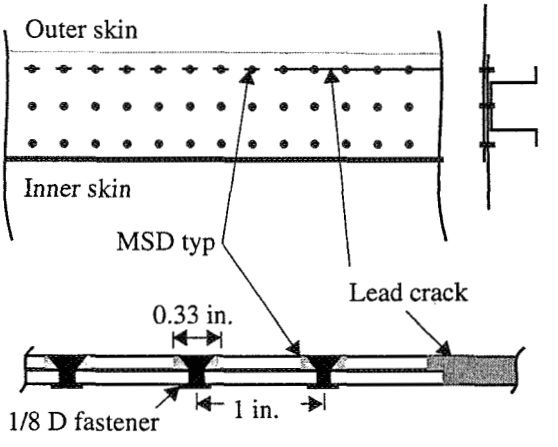

(b) Lap joint detail with lead crack and MSD cracks

Figure 2. Panel ASIP2 prior to testing.

of the lap joint, shown in Fig. 2(b), indicates that the lead crack was along the third row of fasteners in the lap joint. The MSD cracks were introduced prior to panel assembly by making small longitudinal cuts in the outer skin of the lap joint that extend 0.05 in. on each side of the fastener countersink for each fastener in the third row of fasteners. The resulting initial damage state was a 10-in.-long longitudinal lead crack with 0.33-in.-long MSD cracks in the outer skin, spaced ahead of the lead crack with a 1 in. pitch. The lead crack and MSD cracks were defined to be along the 'critical third row of fasteners' which is where lap joint eccentricity, pressure pillowing of the skin, and the fastener countersink combine to promote crack growth in the outer skin.

2.2 PRESSURE-BOX TEST MACHINE AND TEST METHOD

A schematic of the pressure-box test machine is shown in Fig. 3. The pressure-box test machine is capable of applying axial tensile loads of up to 7,000 lb/in. and internal pressure loads of up to 20 psi. Axial loads are applied at each end of the panel by two 225-kip hydraulic actuators connected to curved steel load introduction plates. Pressure is applied to the concave side of the panel using a 100 psi air supply source and a pneumatic control system. Circumferential or hoop loads that develop in the skin of the panel are reacted by flat steel load introduction plates attached to the straight edges of the panel, and two steel rods that connect each load introduction plate to the rigid steel frame of the pressure-box test machine. Hoop loads that develop in the frames of the panel are reacted by steel rods that connect each end of the panel frames to the rigid steel frame of the test machine. Each steel rod that reacts the hoop loads includes a turnbuckle device that can be adjusted to ensure that hoop loads of proper magnitudes are introduced in the panel frames and skin for a given loading condition. The reaction loads in the hoop rods are measured by load cells built into the rods. A continuous rubber seal is connected to the bottom of the axial and hoop load plates and to the top of the steel pressure containment box to permit the panel to float freely when pressurized and to minimize air leakage. A detailed description of this test machine is provided in Ref. 4. The loading condition for the two fuselage panels that were tested was a combination of internal pressure plus axial tension loads. The axial load was prescribed to be equivalent to the bulkhead pressure load in a closed pressurized cylinder, and was applied during the test in proportion to the internal pressure load. Strain gages, linear variable displacement transducers, and video cameras were used to measure the panel response.

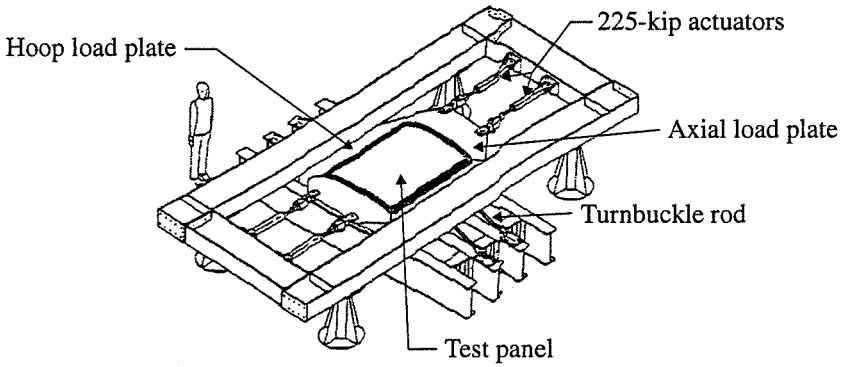

Figure 3. Pressure-box test machine.

2.3 TEST RESULTS

The test results for ASIP1 are summarized in Fig. 4. As the internal pressure was increased, each end of the skin crack extended in the longitudinal direction until it intercepted the adjacent tear strap. The crack growth behavior was symmetric with respect to the central severed frame. A photograph of the entire panel after testing is shown in Fig. 4(a), and a close-up of the crack trajectory on one end of the initial crack is shown in Fig. 4(b). From the video record of the test, it was determined that the crack growth behavior was as indicated on the right side of Fig. 4(b). The initial crack tip location is identified at the bottom of this figure. When the pressure was increased to 14.6 psig, the crack had extended approximately 0.85 in. on each end. At a pressure of 15.9 psig, the crack had extended by 1.95 in. from the initial crack tip location. Then, as the pressure was increased from 15.9 psig to 16.1 psig, the skin crack extended an additional 3.15 in. on each end and then stopped growing when the crack tip propagated to the edge of the adjacent bonded tear strap. The first 1.95 in. of crack growth displayed stable tearing, while the final tearing was marginally stable, extending more than 3 in. over a five second time interval with only a 1.3% increase in load. When the crack growth stopped at the tear straps, the initial 10-in.-long crack had extended to a total length of 20.2 in. and the test was terminated.

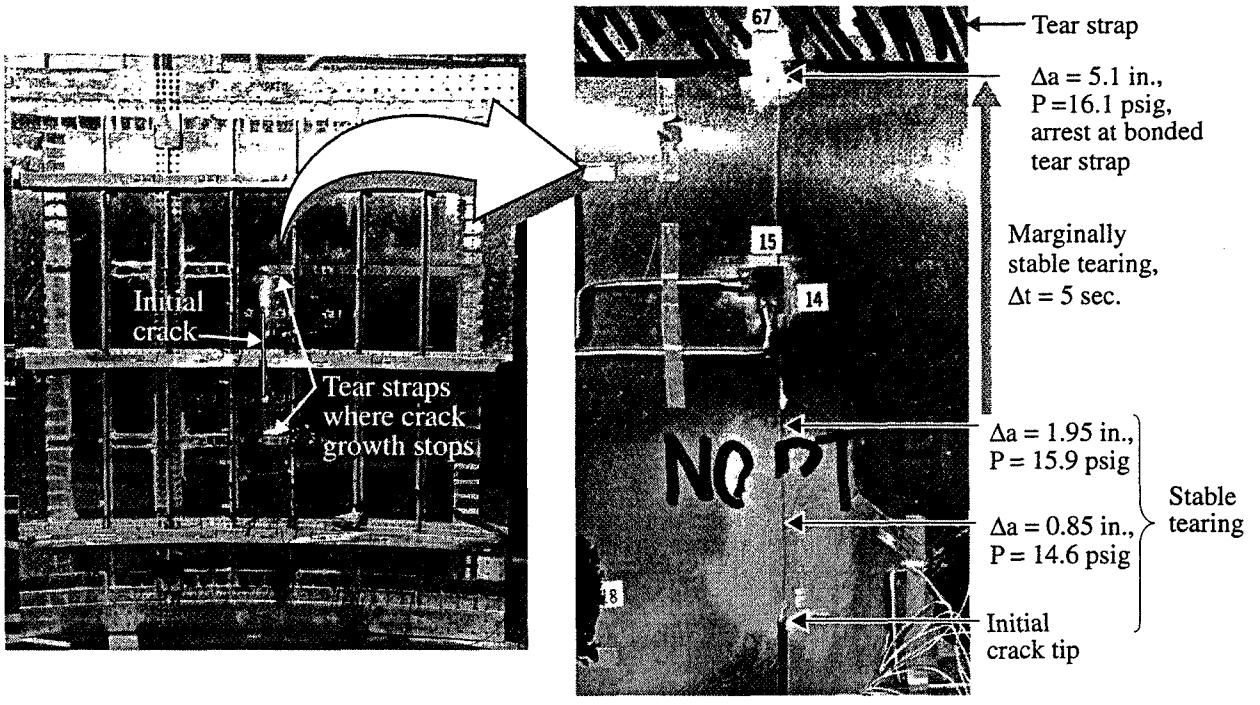

(a) Panel after testing, crack length increased from 10 in. to 20.2 in.

(b) Crack trajectory on one end of the crack

Figure 4. Panel ASIP1 test results.

When panel ASIP2 was tested in the pressure-box test machine, the video record did not show any visible crack growth for pressure levels less than 9.95 psig. When the pressure reached 9.95 psig, the lead crack suddenly extended on each end of the crack, and linked up with the series of MSD cracks ahead of the lead crack. The crack extended in the longitudinal direction in a fast fracture mode, and extended over the entire panel length in an instant. The crack growth behavior was symmetric with respect to the central severed frame. Photographs which characterize the failure of panel ASIP2 are shown in Fig. 5. A view of the outer surface of the panel is shown in Fig. 5(a) which shows that the skin crack has extended the full length of the panel. A view of the inner surface of the panel is shown in Fig. 5(b) which shows that the skin crack has extended past the adjacent frame and tear strap, failing each of these components at fastener hole locations. A close-up of the crack trajectory is shown in Fig. 5(c) which shows the link-up of the MSD cracks along the row of fasteners with the lead crack growing to the right, and the MSD cracks growing to the left and right so that link-up occurs midway between the fasteners.

3. ANALYSES

The analysis method used in the present study to predict the residual strength of stringer- and frame-stiffened aluminum fuselage panels with longitudinal cracks is described in this section. All analyses were conducted using the STAGS (STructural Analysis of General Shells) nonlinear shell analysis code.[1] An overview of the STAGS code and a description of the finite element modeling used are presented. A skin fracture criterion and a method of determining the fracture parameters from small laboratory tests are described. Then, the results of nonlinear analyses of the fuselage panels with damage are presented and compared to the experimental results.

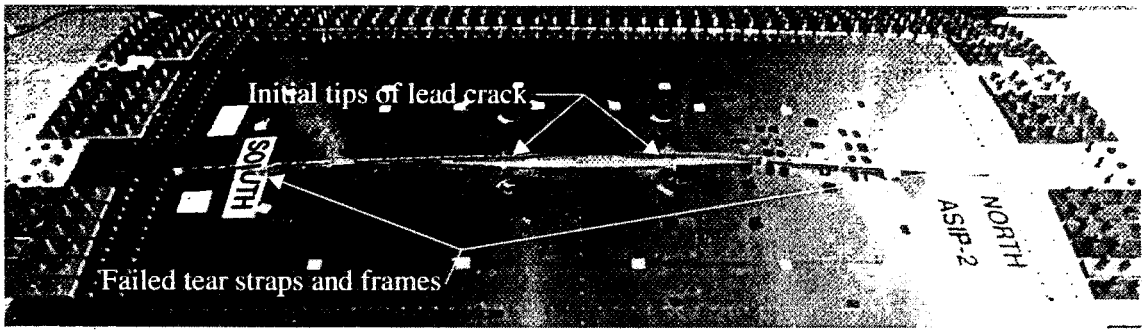

(a) Self-similar crack growth over the entire length of panel, failing adjacent tear straps and frames

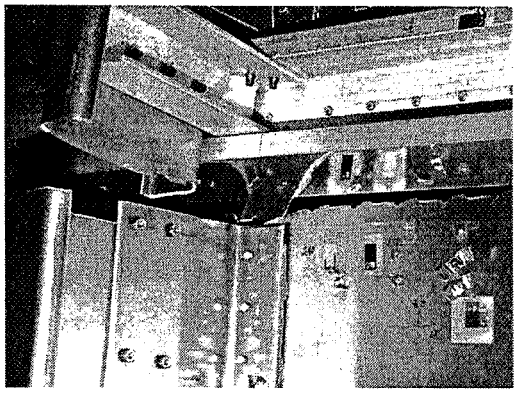

(b) Failed tear strap and frame

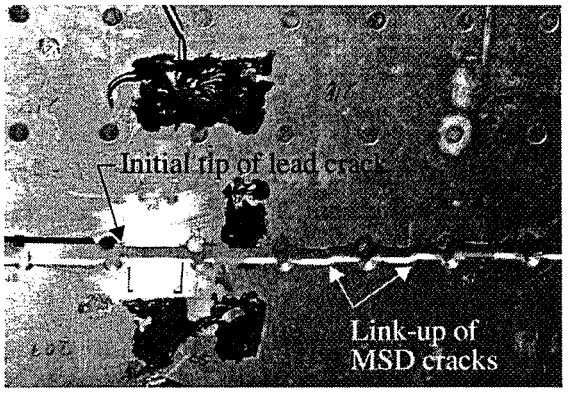

(c) Crack trajectory with link-up of MSD cracks

Figure 5. Panel ASIP2 after testing.

3.1 NONLINEAR ANALYSIS CODE AND FINITE ELEMENT MODELING

STAGS is a finite element code for analyzing general shells and includes the effects of geometric and material nonlinearities in the analysis. The code uses both the modified and full Newton methods for its nonlinear solution algorithms, and accounts for large rotations in a shell by using a co-rotational algorithm at the element level. The Riks pseudo arc-length path following method[5] is used to continue a solution past the limit points of a nonlinear response. The plasticity model in STAGS applies a mechanical sublayer distortional energy plasticity theory. Nonlinear material properties are defined by prescribing a piecewise linear representation of the elastic-plastic stress-strain curve. The material properties of 2024-T3 and 7075-T6 aluminum alloys are given in Fig. 6. The material properties for 2024-T3 are for the T-L orientation since the fuselage test panels have both the sheet rolling direction and the skin cracks parallel to the longitudinal direction.

STAGS can perform crack-propagation analyses, and can represent the effects of crack growth on nonlinear shell response. A nodal release method and a load relaxation technique are used to extend a crack while the shell is in a nonlinear equilibrium state. The changes in the stiffness matrix and the internal load distribution that occur during crack growth are accounted for in the analysis, and the nonlinear coupling between internal forces and in-plane and out-of-plane displacement gradients that occurs in a shell are properly represented. In addition to the nonlinear equilibrium solution, output from STAGS calculations includes the following crack-tip fracture parameters: strain-energy-release rates (used to predict crack growth rates for fatigue loading conditions and residual strength crack extension from an elastic analysis) and the crack-tip-opening angle (CTOA, used to determine residual strength crack extension from an elastic-plastic analysis).

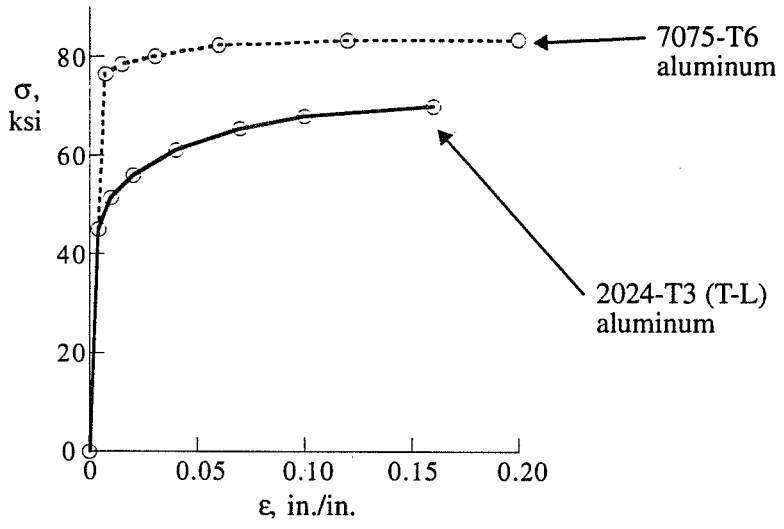

σ, ksi	ε, in./in.
0.00	0.00
76.5	0.0074
78.5	0.015
80.0	0.03
82.3	0.06
83.3	0.12
83.4	0.20

σ, ksi	ε, in./in.
0.0	0.00
45.0	0.0043
51.5	0.01
56.0	0.02
61.0	0.04
65.5	0.07
68.0	0.10
70.0	0.16

Figure 6. Piecewise linear stress-strain curves for 7075-T6 and 2024-T3 (T-L) aluminum alloys.

Procedures for computing the strain-energy-release rates using the modified crack closure integral method, and computing the linear elastic fracture mechanics stress-intensity factors from the strain-energy-release rates are described in Refs. 6-8.

Finite element models are constructed using a collection of two-node beam elements, two-node fastener elements, and four-node plate elements.[9] In addition, five- and seven-node mesh-transition elements which provide 2:1 mesh refinement are used to develop a mesh that has a high level of mesh refinement near the crack and a coarse mesh far away from the crack. Each node of the model has six degrees of freedom. Structural components including skins, stringers, frames, tear straps, and stringer clips are modeled by plate elements to represent accurately the cross sectional shapes of all components.

Riveted connections between structural components are modeled using beam elements, or fastener elements in the region close to a crack, where fastener flexibility is thought to affect load transfer. The fastener elements represent the offsets of the joined components with rigid links that are connected by spring elements with six degrees of freedom. The spring elements can model elastic-plastic behavior, and fastener breakage if a prescribed fastener strength is exceeded. In the fuselage panels considered in the present paper, the fastener loads are relatively low. Thus, in the analyses conducted for the present paper, the fastener elements are assumed to be linear elastic and fastener failure is not considered. The axial, flexural, and torsional stiffnesses of the spring elements are estimated by assuming that the fastener behaves like a simple elastic rod with a diameter equal to the fastener diameter. The elastic shear stiffness of the fastener is computed using the empirical relation developed by Swift,[10]

$$K_s = \frac{ED}{\left[A + C\left(\frac{D}{B_1} + \frac{D}{B_2}\right)\right]}$$

where E is the elastic modulus of the sheet material, D is the fastener diameter, B_1 and B_2 are the thicknesses of the joined sheets, and A and C are empirical factors, equal to 5.0 and 0.8, respectively, for aluminum rivets. This empirical stiffness represents the net shear stiffness of the fastener-sheet connection and accounts for bearing deformations, thus the finite element models do not include modeling of the fastener hole or the countersink details. Also, if the fastener element is joining surfaces with fine meshes, then the fastener load should be distributed to over an area on the surface so that local surface deformations do not reduce the ef-

fective stiffness of the fastener-sheet connection. Load distribution can be accomplished by defining rigid links, beam elements, or a least-squares loading condition to connect the fastener node to the surrounding shell nodes.[11] The area in the shell over which the fastener load is distributed should be of the order of the fastener cross-sectional area, since distributing the load over a larger area may inadvertently stiffen the shell. The bonded tear straps and the skin are modeled as stacked layers in a single shell with the appropriate eccentricity included, thus ignoring any flexibility in the adhesive bond. For conditions where deformation of the model would cause interpenetration of elements, the general contact capability in STAGS is invoked to prevent such penetration.

To simulate the experimental conditions, the finite element models include the load introduction hardware and replicate the loading conditions as applied in the experiments. Symmetry conditions are applied in the model whenever possible to increase the computational efficiency.

3.2 FRACTURE CRITERION

The fracture criterion currently implemented in the STAGS code is the crack-tip-opening-angle (CTOA) criterion. The CTOA criterion is supported by experimental measurements of the critical angle during stable crack growth, and has been shown to be well suited for modeling stable crack growth in ductile materials and predicting the onset of unstable crack growth in fracture analyses conducted using elastic-plastic finite element methods.[2,3] The CTOA is defined as the angle made by the upper crack surface, the crack tip, and the lower crack surface, evaluated at a fixed distance from the moving crack tip, as illustrated in Fig. 7. The CTOA criterion assumes that crack extension will occur when the CTOA reaches a critical value, $CTOA_{cr}$, and that the $CTOA_{cr}$ will remain constant as the crack extends. In a finite element analysis which typically uses two-dimensional plane stress elements, plane strain elements are used in a region on each side of the crack line to simulate the three-dimensional constraint effects developed at the local crack tip.[12] The width of the plane strain region on each side of the crack line is commonly referred to as the plane strain core height, h_c, and is approximately equal to the thickness of the specimen. The parameters $CTOA_{cr}$ and h_c are shown schematically in Fig. 7. The values of $CTOA_{cr}$ and h_c depend on the sheet material, the orientation of the crack relative to the sheet rolling direction, and the sheet thickness, and are determined by correlating elastic-plastic finite element analyses and experimental results for small laboratory specimens.

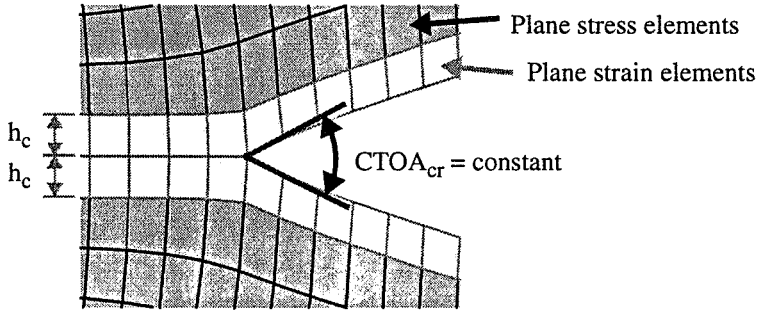

Figure 7. Critical crack-tip-opening angle, $CTOA_{cr}$, and plane strain core height, h_c.

3.3 DETERMINATION OF FRACTURE PARAMETERS

The procedure for determining the values of $CTOA_{cr}$ and h_c from small laboratory specimens for use in the residual strength analyses of the fuselage panels is described. It is assumed that the fracture parameters are a function of the material, sheet thickness, and crack orientation relative to the sheet rolling direction, but are independent of the structural configuration or loading. For the two fuselage panel tests described in the present paper, the skins were 0.063-in.-thick 2024-T3 aluminum alloy with the sheet rolling direction parallel to the panel's longitudinal axis. The skin cracks in each panel are longitudinal cracks, and the principal

stress and yielding in the skin near the crack is in the direction perpendicular to the crack. Thus, the principal stress and yielding in the skin is perpendicular to the sheet rolling direction, which is referred to as the T-L orientation of the material. To determine the fracture parameters for this material and crack orientation, the Mechanics of Materials Branch at NASA Langley Research Center conducted compact tension (C(T)) and middle-crack-tension (M(T)) laboratory tests on 0.063-in.-thick sheets of 2024-T3 aluminum with the cracks parallel to the sheet rolling direction. The compact-tension test was conducted with a 6-in.-wide specimen with an initial crack length a = 2.4 in. Middle-crack-tension tests were conducted for 12-in.-wide and 24-in.-wide specimens with initial crack lengths 2a = 4 in. and 8 in., respectively. These tests included tests where the sheet was constrained against buckling and tests where buckling of the sheet was allowed. Personnel from the Mechanics of Materials Branch then conducted geometrically linear elastic-plastic analyses of the compact-tension test and the middle-crack-tension tests with buckling constrained. Analyses were conducted using three-dimensional elements in the ZIP3D code[13,14] to determine the value of $CTOA_{cr}$ so that ZIP3D analysis results were consistent with the test results. Using three-dimensional elements eliminates the plane stress and plane strain elements required in a two-dimensional analysis, which allows an independent determination of $CTOA_{cr}$. Then, analyses were conducted using two-dimensional elements in the ZIP2D code[15,16] to determine the value of h_c so that ZIP2D analysis results were consistent with ZIP3D results. By following this procedure, personnel of the Mechanics of Materials Branch determined that $CTOA_{cr}$ = 5.0 deg. and h_c = 0.04 in. for 0.063.in.-thick 2024-T3 aluminum for fracture in the T-L orientation.

To confirm that these fracture parameters could be applied in the STAGS analyses, geometrically nonlinear elastic-plastic analyses were conducted to predict the response of the compact-tension and middle-crack-tension panels, with and without buckling constraints. A typical finite element mesh used for analyzing the M(T) panels is shown in Fig. 8. The finite element models utilize mesh refinement to provide an element size of 0.04 in. along the crack line, and utilize symmetry when possible. The experimental and predicted crack extension results for the C(T) and M(T) panels are shown in Fig. 9 as a function of the applied load. These results verify the selection of $CTOA_{cr}$ = 5.0 deg. and h_c = 0.04 in. and indicate that the analyses with STAGS accurately predict the reduction in strength of the panels caused by the geometrically nonlinear effect of panel buckling.

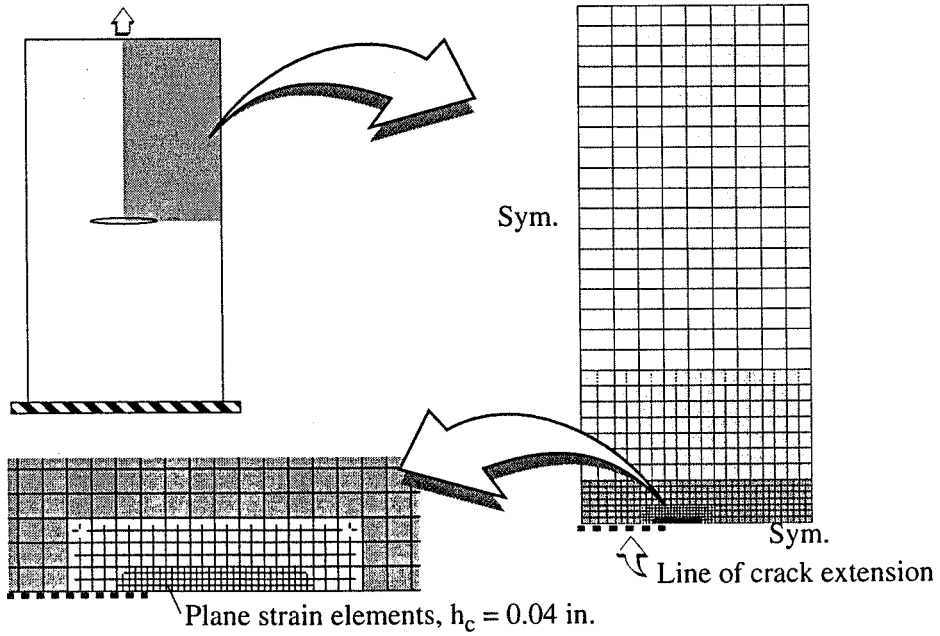

Figure 8. Typical finite element mesh for STAGS analysis of M(T) specimens.

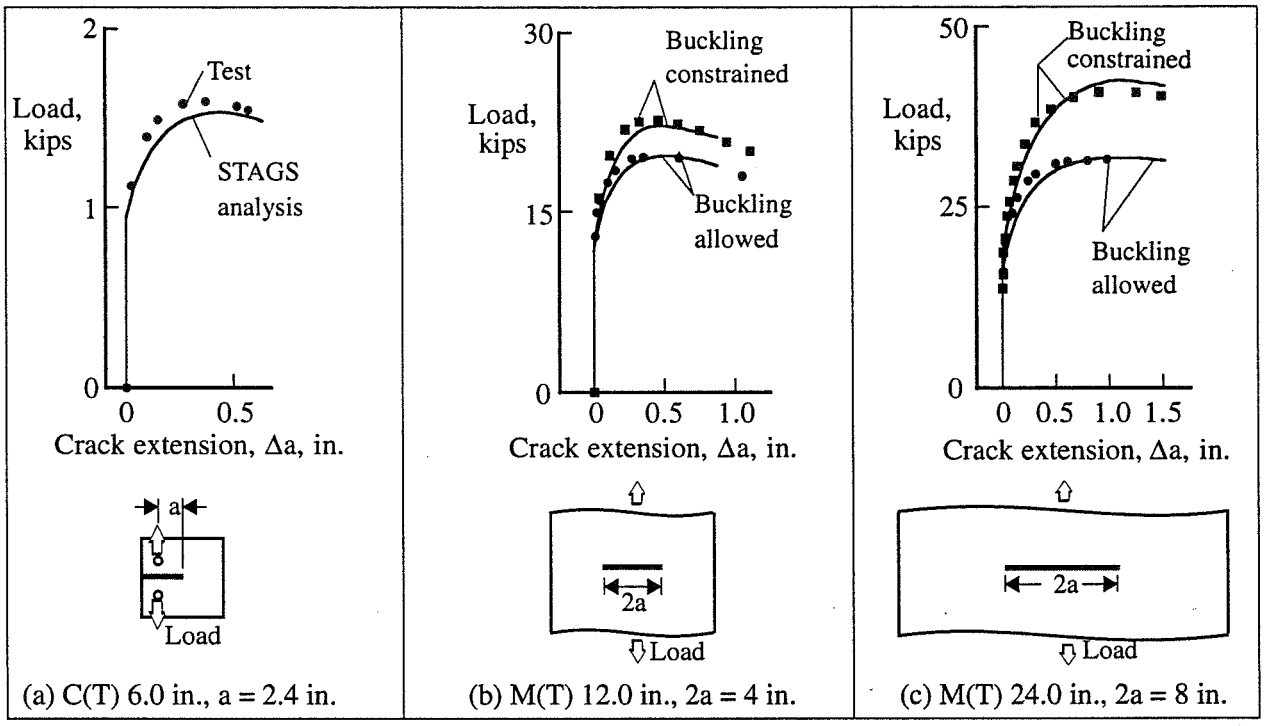

Figure 9. Load versus crack extension results from C(T) and M(T) tests, and nonlinear STAGS analyses with $CTOA_{cr}$ = 5.0 deg. and h_c = 0.04 in.

3.4 FRACTURE ANALYSES OF FUSELAGE PANELS

Geometrically nonlinear elastic-plastic analyses were conducted to predict the residual strength of the two fuselage panels that were tested. In all cases, the element length along the crack is approximately 0.04 in., the region of plane strain elements is defined by h_c = 0.04, and the tearing criterion is $CTOA_{cr}$ = 5.0 deg. The finite element models used for the analyses and results from a typical solution are described. Then, the results of the analyses are compared to the experimental results, with emphasis on the far-field load introduction, the strains in the local region around the crack tip, and the crack extension response as a function of internal pressure.

3.4.1 Fuselage Panel ASIP1

The finite element model for panel ASIP1 has 4,950 elements and 29,300 degrees of freedom, and is shown in Fig. 10. Since this panel has a longitudinal crack that is midway between stringers and is centered on the middle frame, a quarter symmetry model is used for the analysis. The plane of symmetry about the axial direction is located at the center of the middle frame so that only one half of the middle frame cross section is modeled. The plane of symmetry about the hoop direction is located midway between stringers. The asymmetry of the Z-section stringers with respect to this plane is considered to be a small effect and is ignored in the analysis.

A typical solution with 1.0 in. of stable tearing crack extension is shown in Fig. 11. The contour plot of the hoop stress in the region around the crack tip region, shown in Fig. 11(a), indicates a high stress region near the crack tip. A contour plot of the plastic strains in the hoop direction is shown in Fig. 11(b) which indicates the size of the plastic zone around the crack tip, and the existence of a plastic wake which forms behind the moving crack tip as the crack extends.

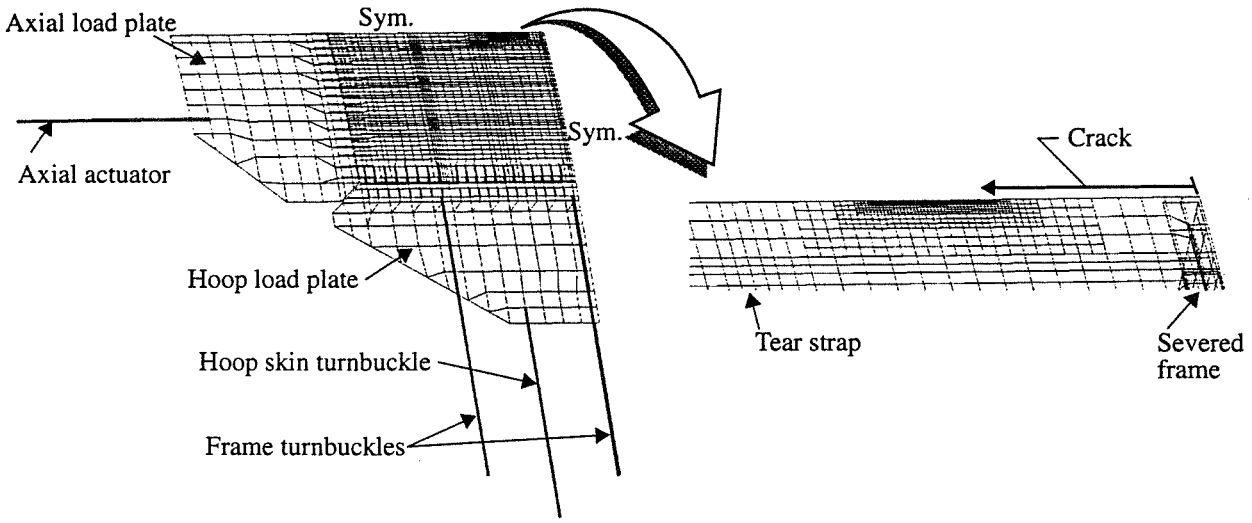

Figure 10. Quarter symmetry finite element model for panel ASIP1.

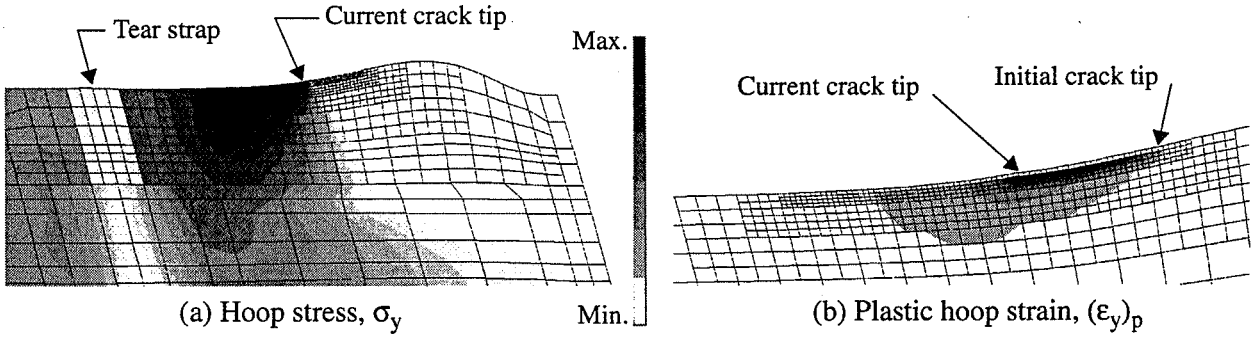

Figure 11. Typical stable tearing analysis results for panel ASIP1 with $\Delta a = 1.0$ in.

The far-field load introduction results predicted by the analysis and measured in the experiment are compared in Fig. 12. The plots of the frame hoop reaction loads and skin hoop reaction loads shown in Figs. 12(a) and 12(b), respectively, indicate good agreement of the results. The predicted and experimental strains in the skin at two locations near the initial crack tip are compared in Fig. 13. The correlation between the predicted and measured skin axial strains and the skin hoop strains shown in Figs. 13(a) and 13(b), respectively, indicates that the finite element model accurately simulates the stress state around the crack tip region.

The crack extension response from the analysis and the experiment is compared in Fig. 14 as a function of pressure. The crack extension data from the experiment were extracted from the video record which did not provide data for crack extension shorter than 0.85 in. These results indicate good agreement in the pressure corresponding to crack extension values of 0.85 in. to 1.0 in., but a discrepancy in the predicted and observed responses occurs for crack extension greater than 1.0 in. In the experiment, after 1.0 in. of crack extension, very small increases in pressure cause significant amounts of crack extension, while the analysis indicates that larger increases in pressure are required for additional crack extension. The values of the pressure for the test and the analysis differ by only 1% for 1 in. of crack extension, but differ by 14% for 2 in. of crack extension. The discrepancy in the nature of the crack growth for crack extension greater than 1.0 in. is consistent with discrepancies that have been observed in test and analysis results of wide unstiffened sheets.

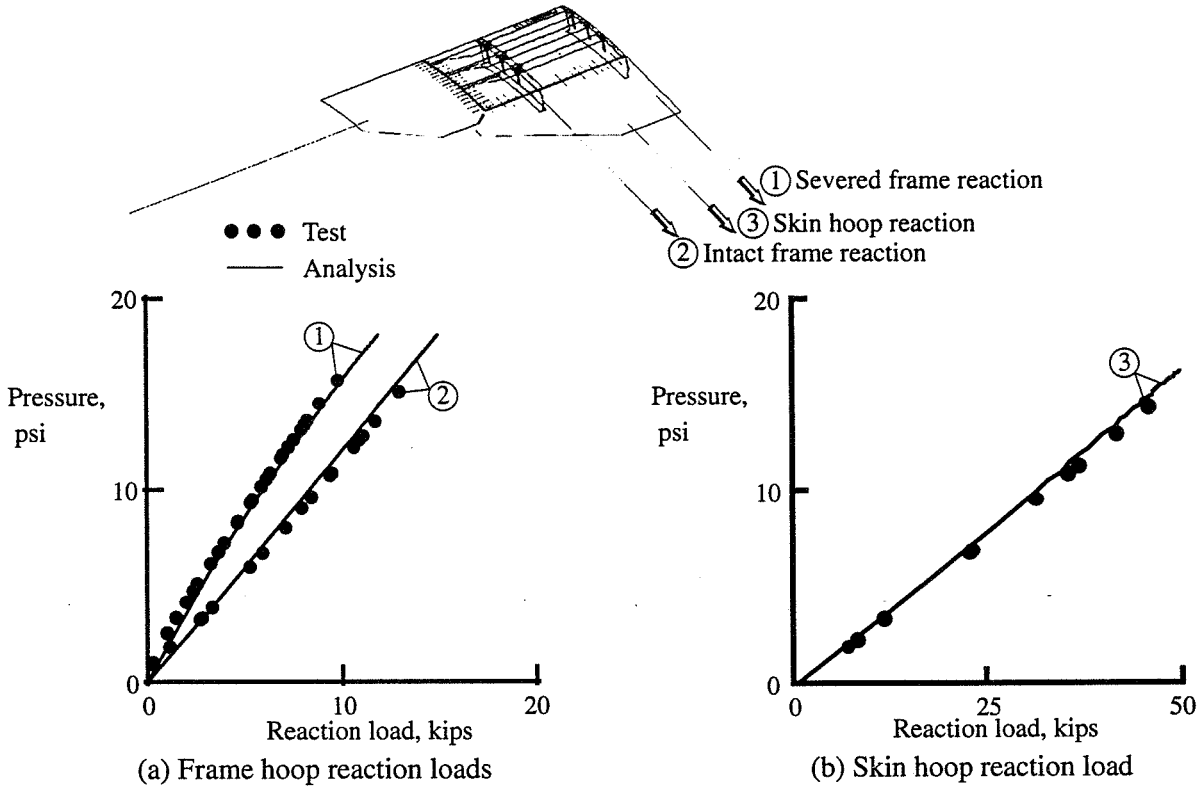

(a) Frame hoop reaction loads (b) Skin hoop reaction load

Figure 12. Panel ASIP1 test-analysis correlation of far-field load introduction results.

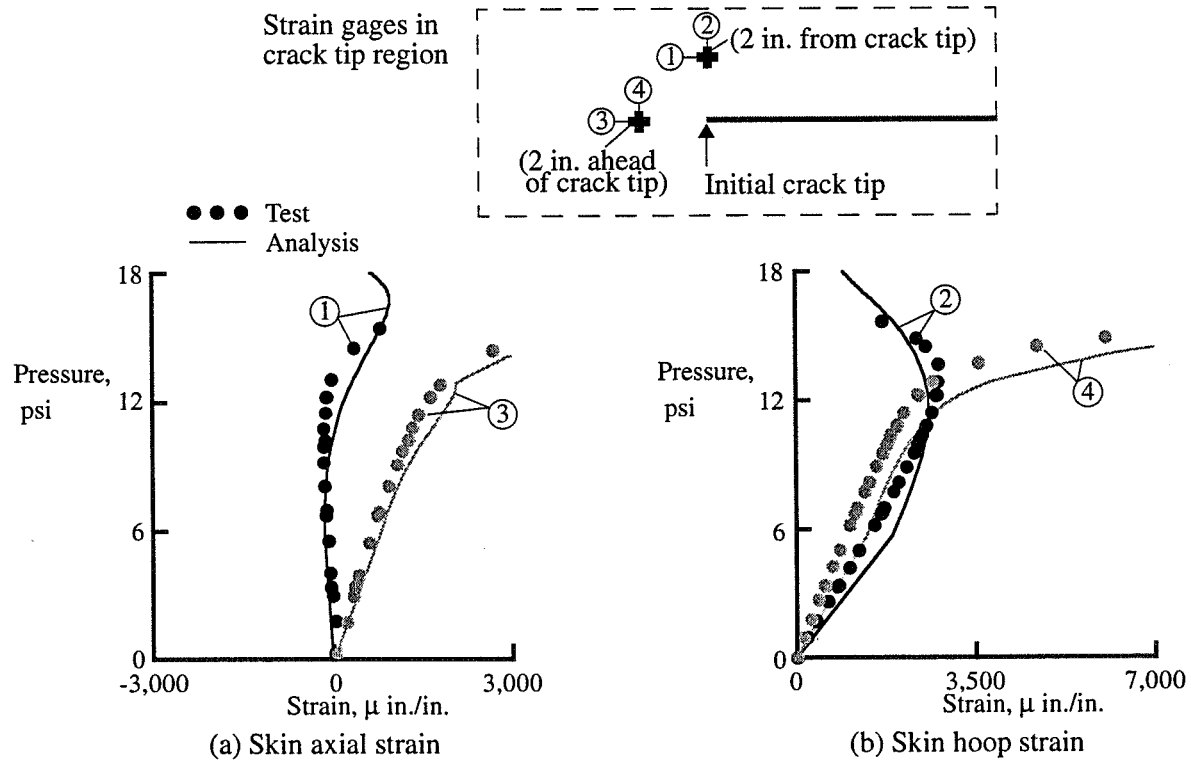

(a) Skin axial strain (b) Skin hoop strain

Figure 13. Panel ASIP1 test-analysis correlation of strain results in a crack tip region.

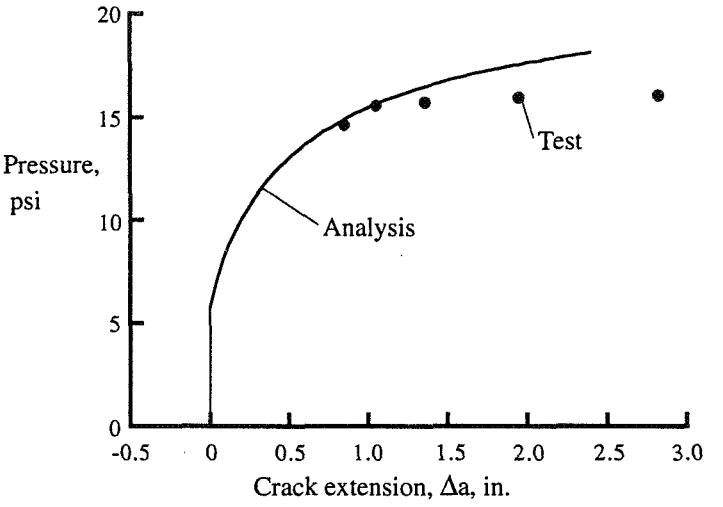

Figure 14. Panel ASIP1 test-analysis correlation of crack extension results as a function of pressure.

3.4.2 Fuselage Panel ASIP2

The finite element model for panel ASIP2 has 11,000 elements and 63,500 degrees of freedom, and is shown in Fig. 15. Since this panel has a longitudinal crack that is adjacent to a stringer and is centered on the middle frame, a half-length symmetry model is used for the analysis. The assumed plane of symmetry about the axial direction is located at the center of the middle frame. To represent the Z-section middle frame, the entire frame cross section is modeled, symmetry conditions are applied to the frame web, and a half thickness is assigned to the frame components. The inner and outer skins of the lap joint are modeled as discrete layered shells connected with fastener elements. Anticipating that panel failure will correspond to link-up of the first few MSD cracks, the MSD cracks are modeled by introducing small cracks in the outer skin at the three fasteners directly ahead of the initial lead crack. In these locations, the fasteners are attached to the side of the crack where compression bearing will occur, and rigid links are used to distribute the fastener connection over a region equal to the rivet cross-sectional area. The general contact capability in STAGS is utilized to prevent penetration of the inner and outer skin layers of the lap joint when the pressure load is applied to the inner skin.

A typical solution with crack growth in the lead crack and the MSD cracks is shown in Fig. 16. The contour plot of the hoop stress in the region around the crack tip region, shown in Fig. 16(a), indicates the high stress regions near the crack tips of the lead crack and the MSD cracks. A contour plot of the plastic strains in the hoop direction is shown in Fig. 16(b) which indicates that there are regions of plastic deformation emanating from the lead crack and from the MSD crack tips, and that for the solution shown, the plastic zones from the lead crack and the first MSD crack have coalesced. The deformed shape shown in these plots indicates that the deformation on the side of the crack attached to the stiffener is much smaller than the deformation on the other side of the crack, demonstrating that the crack is not tearing due to a symmetric loading condition. The asymmetric loading could promote curvilinear crack growth, but it is assumed in the analysis that interaction between the lead crack and the MSD cracks will cause self-similar crack growth. The opening of the MSD cracks is also evident in the deformed shapes.

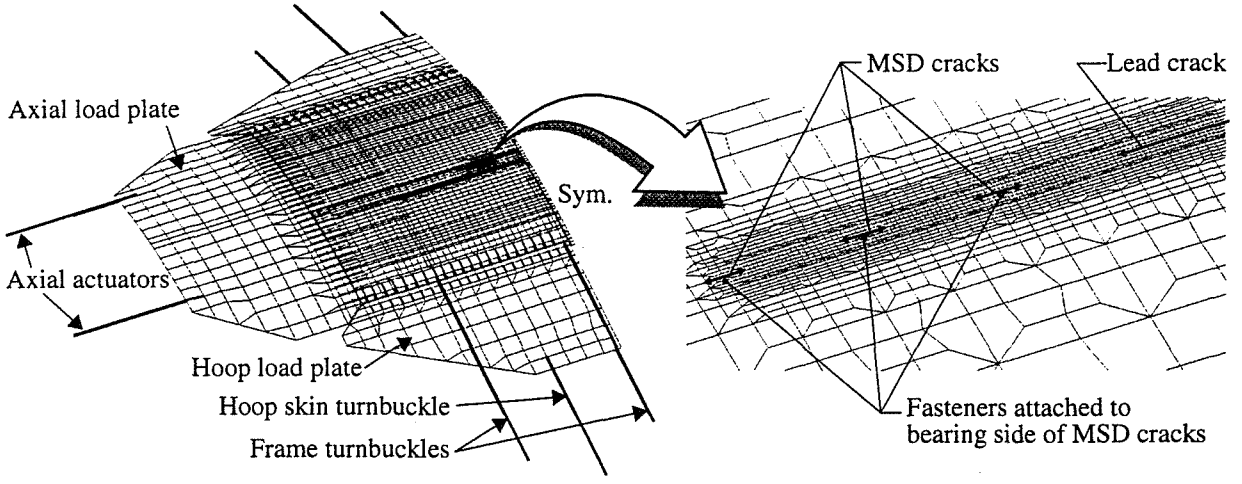

Figure 15. Half-length symmetry finite element model for panel ASIP2.

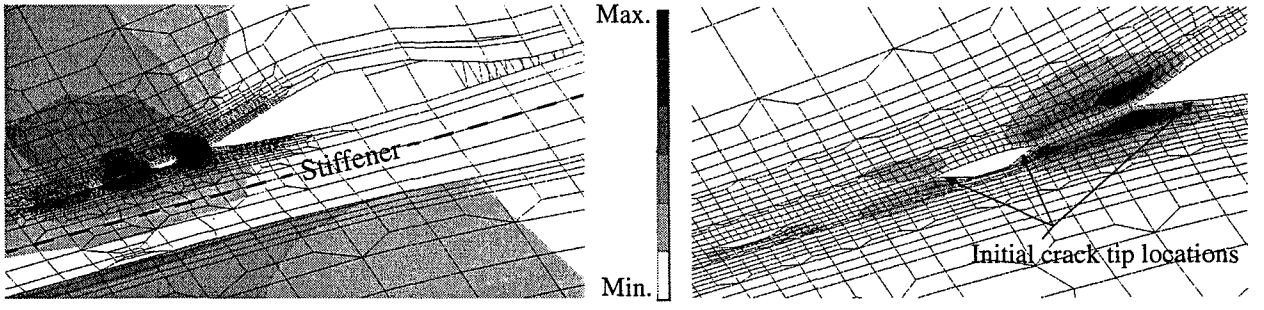

(a) Hoop stress, σ_y (b) Plastic hoop strain, $(\varepsilon_y)_p$

Figure 16. Typical analysis results for panel ASIP2 showing crack growth in the lead crack and MSD cracks.

The far-field load introduction results predicted by the analysis and measured in the experiment are compared in Fig. 17. The plots of the frame hoop reaction loads and skin hoop reaction loads shown in Figs. 17(a) and 17(b), respectively, indicate good agreement of the results. The asymmetry in the frame hoop reactions due to the crack not being in the center of the panel was accurately predicted by the analysis. The predicted and experimental strains in the skin at three locations near the initial crack tip are compared in Fig. 18. The correlation between the skin axial strains and the skin hoop strains shown in Figs. 18(a) and 18(b), respectively, indicates that the finite element model accurately simulates the stress state around the crack tip region.

The crack extension response from the analysis and the experiment are compared in Fig. 19 as a function of pressure. The crack extension data from the experiment are represented by a horizontal line at a pressure of 9.95 psi. The analysis results indicate that a small amount of stable tearing occurs, with a transition to fast fracture occurring at a pressure of 11.01 psi. The breaks in the solid curve indicate locations where the lead crack links up with the MSD cracks to create a discontinuity in the length of the lead crack. Thus, the analysis predicts fast fracture and link-up at a pressure that is 11% greater than what was observed in the experiment. For comparison purposes, the predicted response of panel ASIP1 is also included in Fig. 19. The difference in the predicted stability of the tearing response of these two panels is caused by the interaction of the lead crack and the MSD cracks in panel ASIP2.

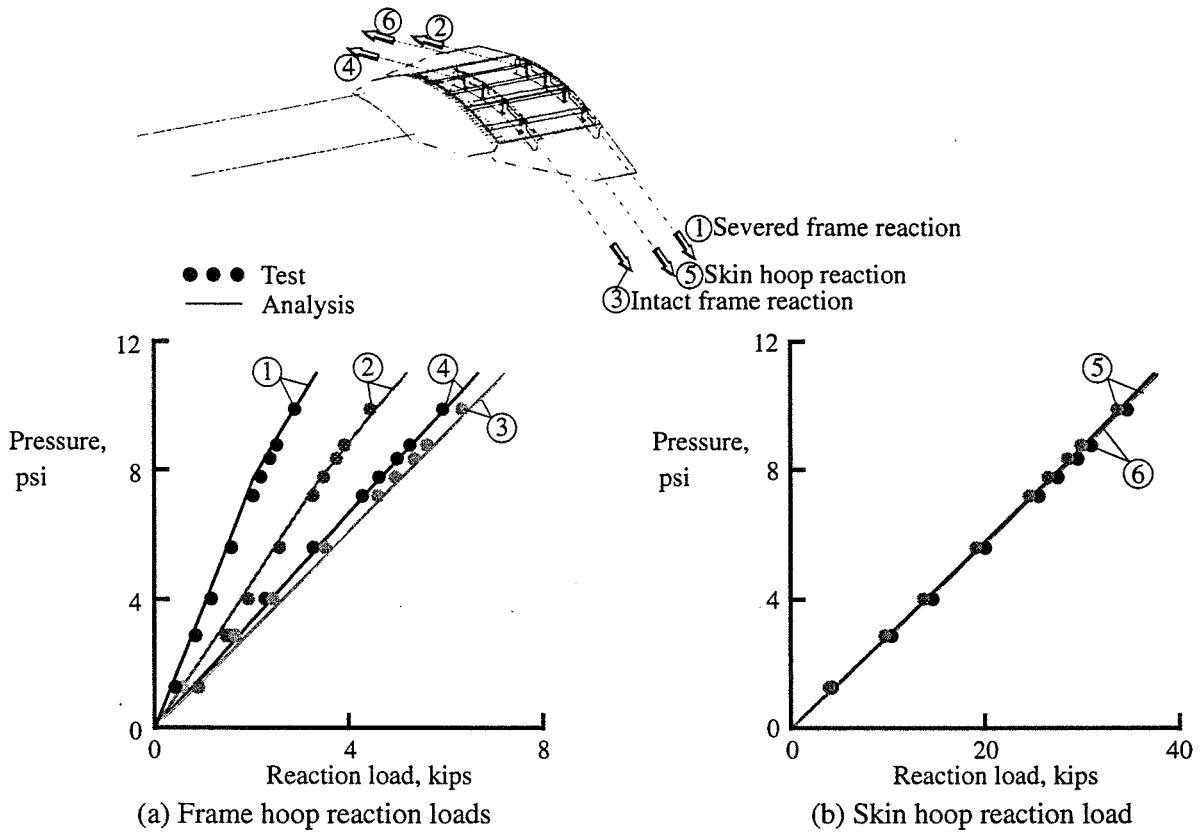

Figure 17. Panel ASIP2 test-analysis correlation of far-field load introduction results.

To illustrate the effect of the MSD cracks on the stable tearing response, additional analysis results are presented which isolate the crack extension behavior of the lead crack and the MSD cracks. The extensions of crack tips 1, 2, and 3 are plotted as a function of pressure in Fig. 20, where crack tip 1 is the crack tip of the lead crack, crack tip 2 is the crack tip of the first MSD crack on the end closest to the lead crack, and crack tip 3 is the crack tip on the other end of the first MSD crack. At a point in the solution corresponding to Point (A) in the plot, the pressure is 9.28 psi and stable tearing has initiated at the lead crack, crack tip 1. The plastic strain in the hoop direction that corresponds to Point (A) is shown in Fig. 20(b), and indicates that plastic strains are most apparent at the tip of the lead crack, but a small region of yielding exists at crack tip 2 in the MSD crack. At Point (B) in the solution, the pressure is 10.68 psi, and stable tearing occurs at crack tip 1 and crack tip 2. The plot of the plastic strains at Point (B) indicates that the plastic zones at crack tip 1 and crack tip 2 have coalesced, and that yielding has initiated at crack tip 3. At Point (C) in the solution, the pressure is 11.01 psi, and the tearing at crack tip 1 and crack tip 2 has become unstable as the two crack tips grow toward each other at a constant pressure. The plot of the plastic strains at Point (C) indicates that a large amount of yielding has occurred between crack tip 1 and crack tip 2, and additional yielding has occurred at crack tip 3. At Point (D) in the solution, the pressure remains at 11.01 psi, crack tip 1 and crack tip 2 have coalesced, and the lead crack has suddenly extended from crack tip 1 to crack tip 3. At this point, crack tip 3 is also displaying unstable crack growth toward the next MSD crack, which is also growing toward crack tip 3. At a constant pressure of 11.01 psi, the MSD cracks will continue to grow toward each other and the panel will tear along the row of MSD cracks until the crack intersects a tear strap or frame which may, or may not, arrest the propagating crack. In the experiment, the running crack caused the tear straps and frames to overload and fail, and the skin crack propagated to the ends of the panel.

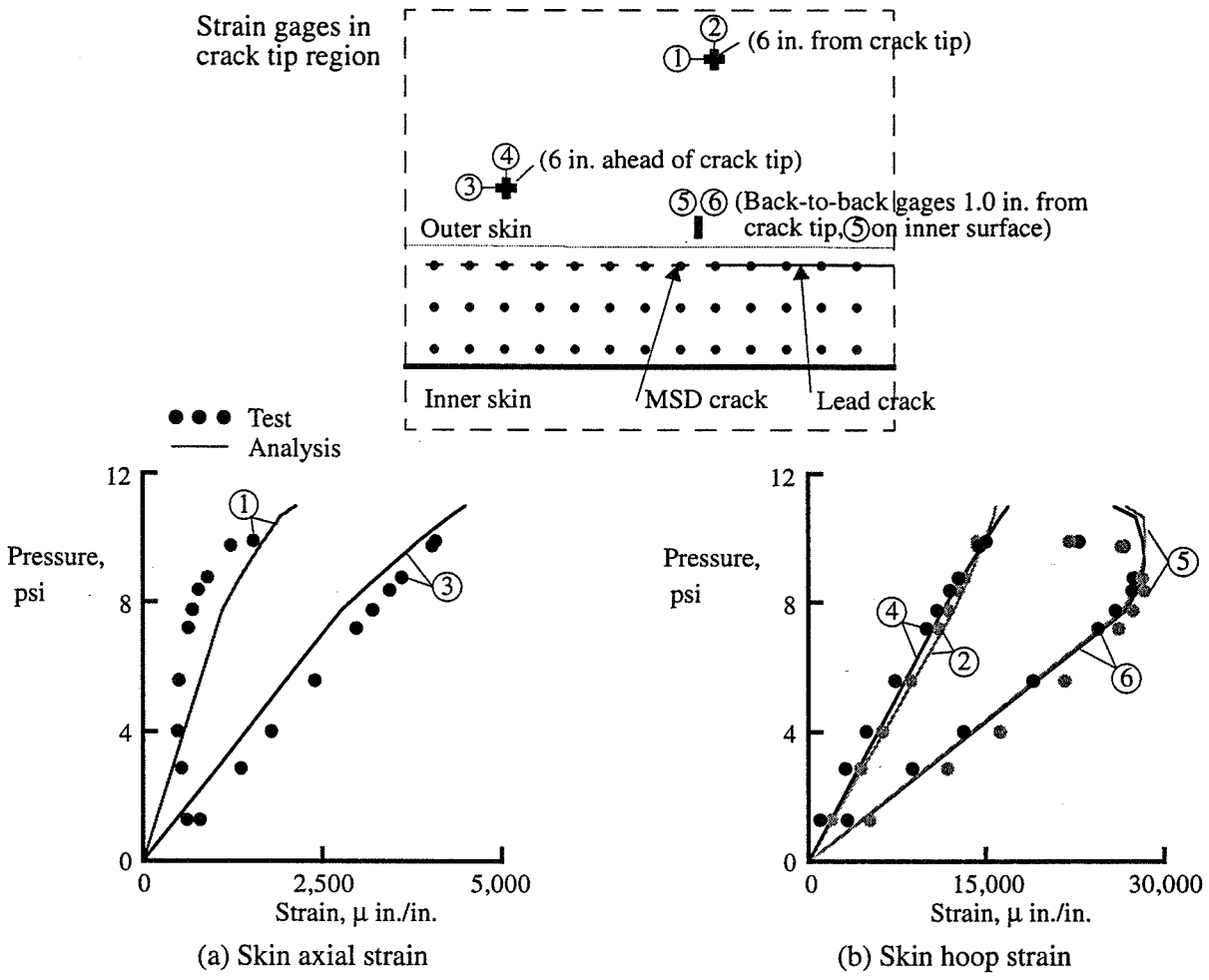

Figure 18. Panel ASIP2 test-analysis correlation of strain results in a crack tip region.

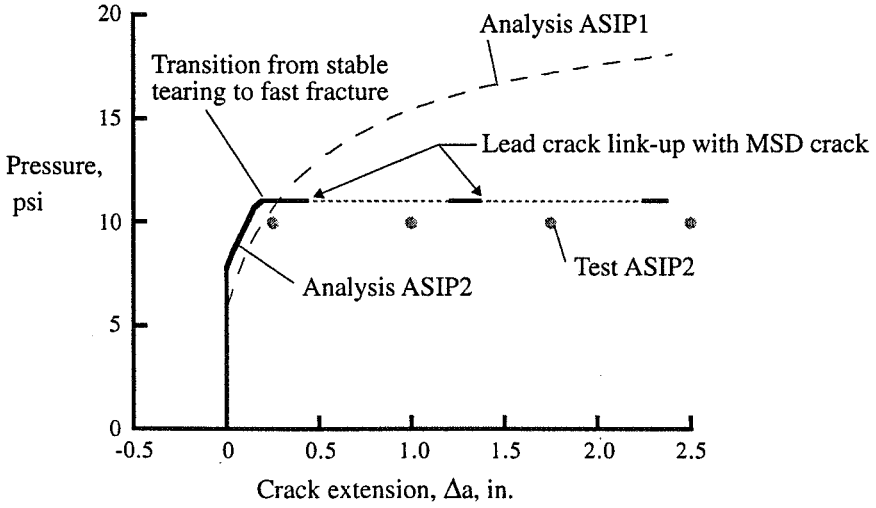

Figure 19. Panel ASIP2 test-analysis correlation of crack extension results as a function of pressure.

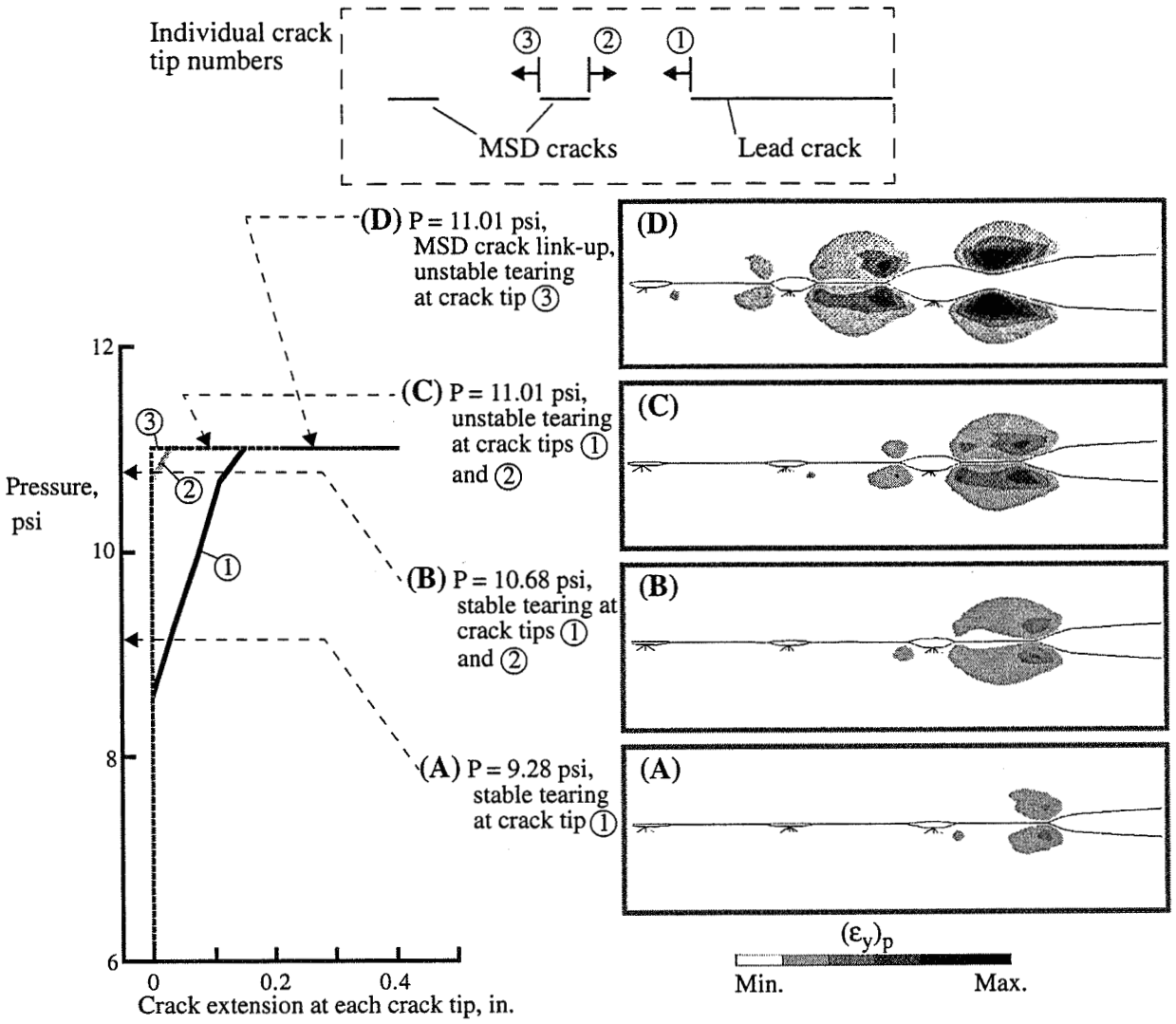

(a) Crack extension as a function of pressure

(b) Plastic strain in the hoop direction at solutions corresponding to points (A), (B), (C), and (D)

Figure 20. Crack extension behavior of the lead crack and the MSD cracks.

CONCLUDING REMARKS

Results of residual strength pressure tests and nonlinear analyses of two stringer- and frame-stiffened aluminum fuselage panels with longitudinal cracks have been presented. Both fuselage panels were generic wide-body fuselage panels with 0.063-in.-thick 2024-T3 aluminum skins. The first fuselage panel had six stringers and three frames, and circumferential tear straps located midway between the frames. The initial damage for this panel was a 10-in.-long longitudinal crack, located midway between stringers and centered on a severed frame. The second fuselage panel had four stringers and three frames, and waffle tear straps located under the stringers and frames. The initial damage for the second fuselage panel consisted of a 10-in.-long longitudinal lead crack and multiple-site damage (MSD) cracks, located adjacent to a stringer, along the edge of a lap joint, and centered on a severed frame.

For the fuselage panel with the lead crack located midway between stringers and no MSD cracks, a substantial amount of stable tearing occurred, and the tear straps located midway between the frames arrested the crack growth in the skin. For the panel with the lead crack and MSD cracks adjacent to a stringer and along a lap joint, very little stable tearing occurred. Interaction between the lead crack and the MSD cracks caused unstable crack growth that could not be arrested by the panel to occur at a relatively low pressure load. For both panels considered, there was significant out-of-plane deformation along the crack, indicating a geometrically nonlinear response. For the case with the lead crack adjacent to a stringer, the deformations were not symmetric across the crack, indicating a mixed-mode loading condition at the crack tip. The numerical and experimental results presented in the paper support the following general remarks. The difference in the crack growth behavior and the residual strength of the two panels implies that the presence of MSD cracks affects the crack growth stability and reduces the residual strength of stiffened fuselage shells with long cracks. Also, the arrest of the crack growth at the tear strap in the first panel, and the failure of the tear straps and frames at fastener hole locations in the second panel, suggest that the tear strap location and sizing, and methods of attaching the skins, tear straps, and stiffening structure may affect the ability to arrest crack growth.

The results presented in the paper show that geometric and material nonlinear structural analyses can accurately represent the internal load distributions, local stress and displacement gradients, and crack growth behavior in stiffened fuselage shells with long cracks and subjected to internal pressure loads. The nonlinear structural analysis methods provide higher fidelity results than traditional linear-elastic engineering analysis approximations for these panel configurations which display significant plastic yielding and nonlinear out-of-plane deformations. To obtain good correlation of test and analysis results for built-up fuselage shell structures, it may be necessary to include all structural detail features and nonlinear response characteristics (e.g., element or component buckling, contact, and fastener yielding or failure) in the numerical models. The numerical models and structural analysis methods must be able to represent accurately the multiple length scales involved in simulating the global response of a large stiffened panel, the local fracture behavior of thin sheets, and the interaction between structural components and load redistribution in a stiffened structure as the damage propagates.

ACKNOWLEDGMENTS

The authors would like to express their thanks to Mr. David F. Moore, Analytical Services and Materials, Inc., and Mr. Roland F. Vause, NYMA, Inc., for their technical support.

REFERENCES

[1]Rankin, C. C., Brogan, F. A., Loden, W. A., Cabiness, H. D., "STAGS User Manual, Version 3.0," Lockheed Martin Missiles and Space Co., Inc., Advanced Technology Center, Report LMMS P032594, June, 1998.

[2]Newman, J.C., Jr., "An Elastic-Plastic Finite Element Analysis of Crack Initiation, Stable Crack Growth, and Instability," ASTM STP 833, 1984, pp. 93-117.

[3]Dawicke, D. S., Sutton, M. A., Newman, J. C., Jr., and Bigelow, C. A., "Measurement and Analysis of Critical CTOA for an Aluminum Alloy Sheet," NASA TM-109024, September 1993.

[4]Ilcewicz, L. B., Smith, P. J., and Horton, R. E., "Advanced Composite Fuselage Technology," NASA CP-3178, 1992, pp. 97-156.

[5]Riks, E., "Some Computational Aspects of the Stability Analysis of Nonlinear Structures," Computational Methods in Applied Mechanics and Engineering, Vol. 47, 1984, pp. 219-259.

[6]Rankin, C. C., Brogan, F. A., and Riks, E., "Some Computational Tools for the Analysis of Through Cracks in Stiffened Fuselage Shells," Computational Mechanics, Springer International, Vol. 13, No. 3, December 1993, pp. 143-156.

[7]Potyondy, D. O., "A Software Framework for Simulating Curvilinear Crack Growth in Pressurized Thin Shells," Ph.D. Thesis, Cornell University, Ithaca, NY, 1991.

[8]Potyondy, D. O., Wawrzynek, P. A., and Ingraffea, A. R., "Discrete Crack Growth Analysis Methodology for Through Cracks in Pressurized Fuselage Structures," International Journal for Numerical Methods in Engineering, Vol. 38, 1995, pp. 1611-1633.

[9]Rankin, C. C., and Brogan, F. A., "The Computational Structural Mechanics Testbed Structural Element Processor ES5: STAGS Shell Element," NASA CR-4358, 1991.

[10]Swift, T., "Fracture Analysis of Stiffened Structure," In Damage Tolerance of Metallic Structures: Analysis Methods and Application, ASTM STP 842, 1984, pp. 69-107.

[11]Young, R. D., Rose, C. A., Dávila, C. G., Starnes, J. H., Jr., and Rankin, C. C., "Crack Growth and Residual Strength Characteristics of Selected Flat Stiffened Aluminum Panels," Proceedings of the First Joint DoD/FAA/NASA Conference on Aging Aircraft, Ogden, UT, July, 1997.

[12]Dawicke, D. S., Newman, J.C., Jr., and Bigelow, C. A., "Three-Dimensional CTOA and Constraint Effects During Stable Tearing in a Thin-Sheet Material," In Fracture Mechanics: 26th Volume, ASTM STP 1256, 1995, pp. 223-242.

[13]Shivakumar, K. N. and Newman, J. C., Jr., "ZIP3D - An Elastic-Plastic Finite-Element Analysis Program for Cracked Bodies," NASA TM-102753, 1990.

[14]Dawicke, D. S. and Newman, J. C., Jr., "Residual Strength Predictions for Multiple Site Damage Cracking Using a Three-Dimensional Finite Element Analysis and a CTOA Criterion," Fatigue and Fracture Mechanics: 29th Volume, ASTM STP 1332, T. L. Panontin and S. D. Sheppard, Eds., American Society for Testing and Materials, 1998.

[15]Newman, J. C., Jr., "Finite Element Analyses of Fatigue Crack Propagation -- Including the Effects of Crack Closure," Ph.D. Thesis, Virginia Polytechnic institute and State University, Blacksburg, VA, May 1974.

[16]Dawicke, D. S., "Residual Strength Predictions Using a Crack Tip Opening Angle Criterion," FAA-NASA Symposium on the Continued Airworthiness of Aircraft Structures, DOT/FAA/AR-97/2, Vol. II, July 1997, pp. 555-566.